Composites Communications 19 (2020) 142–146

Contents lists available at ScienceDirect

Composites Communications

journal homepage: www.elsevier.com/locate/coco

Fabrication of thermoplastic functionally gradient composite parts with anisotropic thermal conductive properties based on multicomponent fused deposition modeling 3D printing

Jianlei Wang [a], Suhail Mubarak [a,c], Duraisami Dhamodharan [a,c], Nidhin Divakaran [a,c], Lixin Wu [a,**], Xu Zhang [b,*]

[a] CAS Key Laboratory of Design and Assembly of Functional Nanostructures, And Fujian Key Laboratory of Nanomaterials, Fujian Institute of Research on the Structure of Matter, Chinese Academy of Sciences, Fuzhou, Fujian, 350002, PR China
[b] Innovation Center for Textile Science and Technology, Donghua University, Shanghai, 201620, PR China
[c] University of Chinese Academy of Sciences, Beijing, 100049, PR China

ARTICLE INFO

Keywords:
Functionally gradient materials
Thermal conductivity
Fused deposition modeling
3D printing

ABSTRACT

A multicomponent fused deposition modeling 3D printing approach was proposed to fabricate thermoplastic functionally gradient composite parts (TFGCPs). The thermal conductive properties of the fabricated TFGCPs were studied by slice and as integrate, respectively. The variation of thermal conductivity by slice versus the number of layer shows that the curve of PCL/AlN has a constant slope, while the one of PCL/BN first increases and then decreases. It is attributed to that the network of thermal conduction is constructed when the loading of BN particles approaches 27wt%, leading to a substantial growth in thermal conductivity. The thermal conductivity of the TFGCPs as integrate lies between the one of pure PCL and homogeneous composite parts with AlN or BN fillers and has a relationship with the filler loading direction exhibiting thermal anisotropy. This study establishes the relationship between properties and structures of thermoplastic functionally gradient composite parts, which helps to lay a theoretical foundation of applications as intermediate layers.

1. Introduction

Functionally gradient materials (FGMs) are consisted of a synergistic combination of different materials, which, unlike the conventional coating materials, can achieve a corresponding change in composition between the respective end members as well as properties [1]. With the latest advances, the FGMs presented by Japanese scholars in the late 1980s are developing at an incredible pace in the speed and have compressive applications, ranging from aeronautics and biomedicine to mechanical engineering optics and energy area, which shows high potential in special application fields [2–4]. The advancements of the FGMs are focused on the design, the preparation, and the evaluation of materials, among which the design is the foundation and defines the composition of materials and the distribution of structure gradient according to different application scenarios. While the preparation determines the possibility of achievement of design and the property of materials, playing the crucial role in the whole process [5].

Additive manufacturing (AM) has unparalleled advantages in the speed and accuracy of printing models with complex geometries and low manufacturing cost, which has represented a new edge on prototyping process evolution and captured the world's horizon nowadays [6–9]. Fused deposition modeling (FDM) invented and developed by Stratasys Inc. in the early 1990s is the trendiest technique among all AM technologies, showing high potentials for fabricating thermoplastic parts with the capacity to compete with conventional processing techniques [10,11]. Due to the characteristic of FDM process that the feeding and printing proceed simultaneously, it is possible to adjust the kind and proportion of feedstock at any time during the printing process. Some scholars prepared fiber reinforced thermoplastic composites via modified methodology of FDM and studied the relationship between structures and properties, which further broadens the engineering applications of FDM [12–14]. While other scholars developed the functional applications of FDM by adding fillers into matrix, including magnetic [15], thermal conductive [11,16], and electric conductive

* Corresponding author.
** Corresponding author.
E-mail addresses: lxwu@fjirsm.ac.cn (L. Wu), xuzhang@dhu.edu.cn (X. Zhang).

https://doi.org/10.1016/j.coco.2020.03.012
Received 8 November 2019; Received in revised form 6 March 2020; Accepted 20 March 2020
Available online 23 March 2020

properties [17]. In the present study, the feeding system and modified the nozzle was designed for FDM process to prepare thermoplastic functionally gradient composites with thermal anisotropy. Also, the thermal conductive properties of the fabricated samples were studied by slice and as a whole and then the relationship between properties and structure of thermoplastic gradient composite parts was further explored, which established theoretical basis for further applications.

2. Experimental section

Three different powders were adopted, including aluminium nitride (AlN) with 30 μm in particle size and boron nitride (BN) with 30 and 10 μm in particle size. For convenience, the 30 μm AlN, 30 μm BN, and 10 μm BN was denoted by AlN-30, BN-30, and BN-10 in the following, respectively. To satisfy the requirements of FDM process, choosing polymer matrix to bond powders is very important. In that case, we developed the modified polycaprolactone (PCL) named Polymate based on Capa™ 6500 produced by Perstorp Co. to fit for FDM process, whose melting point was about 60 °C [18]. It has low linear heat shrinkage rate, so the fabricated parts have no warpage and accurate dimensional stability. The materials were heated and squeezed by two channels in the heating chamber. When they came into merging area, the amount was very small. The heating temperature was set at 100 °C during printing process, which decreased the viscosity to a certain degree. Meanwhile, polymer will be shorn and squeezed by the wall when it comes out of the nozzle. As a result, two components can be mixed well. The Izod notched impact strength was tested according to ASTM D256 and implemented in Instron Ceast 9050. The thermal conductivity of homogeneous specimens was measured by transient hot-wire method, following the ISO 22007 standard. While the one of inhomogeneous specimens was evaluated by steady-state heat flow method, following the ASTM D5470 standard. The SEM fractured surface micrographs were taken with Hitachi SU8010 FEG-SEM with an acceleration voltage of 5 kV after the specimens were fractured in liquid nitrogen. The additional experiment details have been incorporated into the Supporting Information (S1, S2, and S3).

3. Results and discussion

In order to acquire excellent thermal conductive properties for the materials, high content of fillers is requisite. However, there exists an upper limit of filler loading for printable filament for FDM 3D printing. As shown in Scheme S3 (see the Supporting Information), the filaments are squeezed by the driving gear and driven wheel and then fed into the heating chamber, which means that the materials need deformability and toughness to a certain degree. According to the shape and the size of fillers, it revealed that the upper limit of filler content for FDM 3D printing process was different, showing 70 wt% for AlN-30, 50 wt% for BN-30, and 40 wt% for BN-10, respectively. Fig. 1a indicates the variation of notched impact strength of injection molding samples with different fillers following IZOD impact test. The critical value of the materials suitable for FDM 3D printing is around 3 MPa, which was acquired after hundreds of experiments. When introducing slight AlN-30, the notched impact strength increases slightly, peaking at 20 wt%. It can be attributed to that the AlN-30 particles regarded as the nucleating agent accelerate the crystallization process and decrease the degree of crystallinity of the PCL matrix [19,20]. Also, the AlN-30 particles are circular in shape shown in Fig. 1b and c, working similarly as reinforcing materials, such as TiO_2 [21]. However, there exhibits a different trend when adding BN, which is mainly due to the planar shape of BN, as shown in Fig. 1d and e, leading to brittleness of the composites. It can be seen that the notched impact strength decreases dramatically as filler content reaches 40 wt% under all circumstances, which coincides with the experimental phenomenon that the surface is coarse with granular sensation. It can be explained that the agglomeration is severe when the content of particle increases to a certain degree. There are many voids

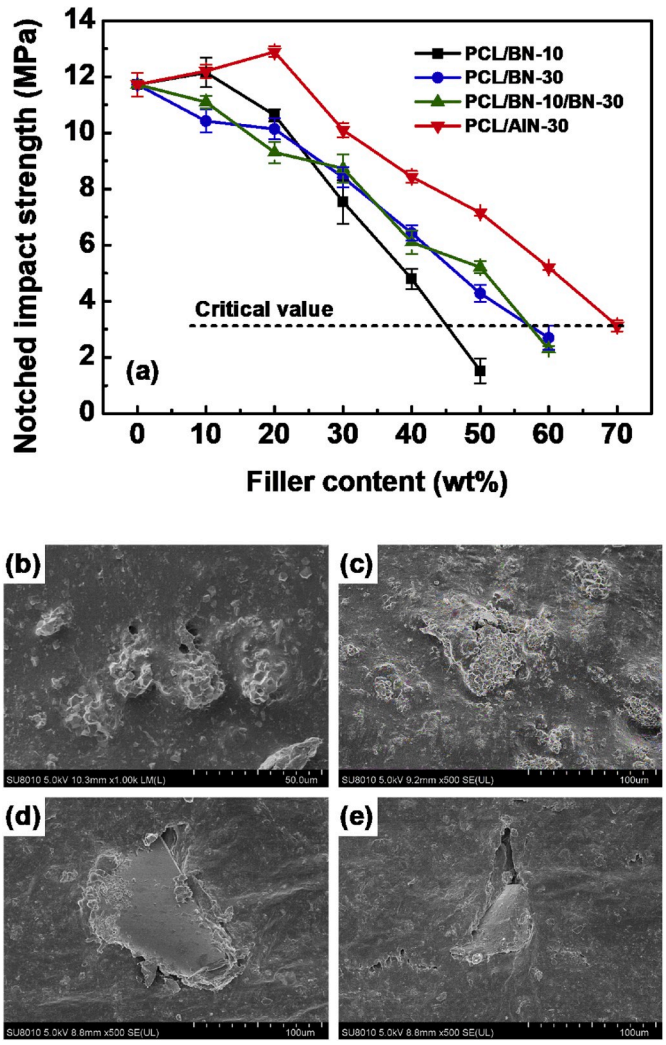

Fig. 1. (a) The effect of filler loading on notched impact strength of injection molding specimens with different fillers following IZOD impact test. The weight percentage of BN-10 and BN-30 in the PCL/BN-10/BN-30 composites (olive line) is equal (i.e. 1:1). The SEM of fracture interface of samples with (b, c) AlN-30, (d) BN-30, and (e) BN-10.

between matrix and particles and thus the matrix can't bond particles effectively.

As shown in Fig. 2a, the influence of filler content on thermal conductivity is significant, indicating that the more thermal conductive filler leads to the better thermal conductivity. When introducing 70 wt% of AlN-30 particles, the thermal conductivity reaches 1.543 W m^{-1} K^{-1}, comparing to 0.233 W m^{-1} K^{-1} of pure PCL. This is mainly due to that the AlN-30 particles have ordered lattice structure with high thermal conductivity and replace PCL molecules in some place. While the lattice vibration mainly results in thermal conduction in PCL, which is hindered by molecular entanglement and incomplete lattice [22]. However, the curves for the samples with BN powders are entirely above the samples with AlN-30, observing 2.463 m^{-1} K^{-1} in thermal conductivity when adding 50 wt% of BN-30 powders. It is likely that the BN particles, which have a planar shape, allow a favorable filler packing and network formation, as illustrated in Fig. 2b, thus providing facile heat dissipation in the in-plane direction of the composites [23]. Also, the orientation of BN particles will occur in the extrusion process of FDM 3D printing process, which leads to increase in particle contact point and decrease in interface resistance. The IRT photography of samples with the passage of time could further demonstrate the difference of thermal conductivity of three kinds of samples vividly, as presented in Fig. 2c.

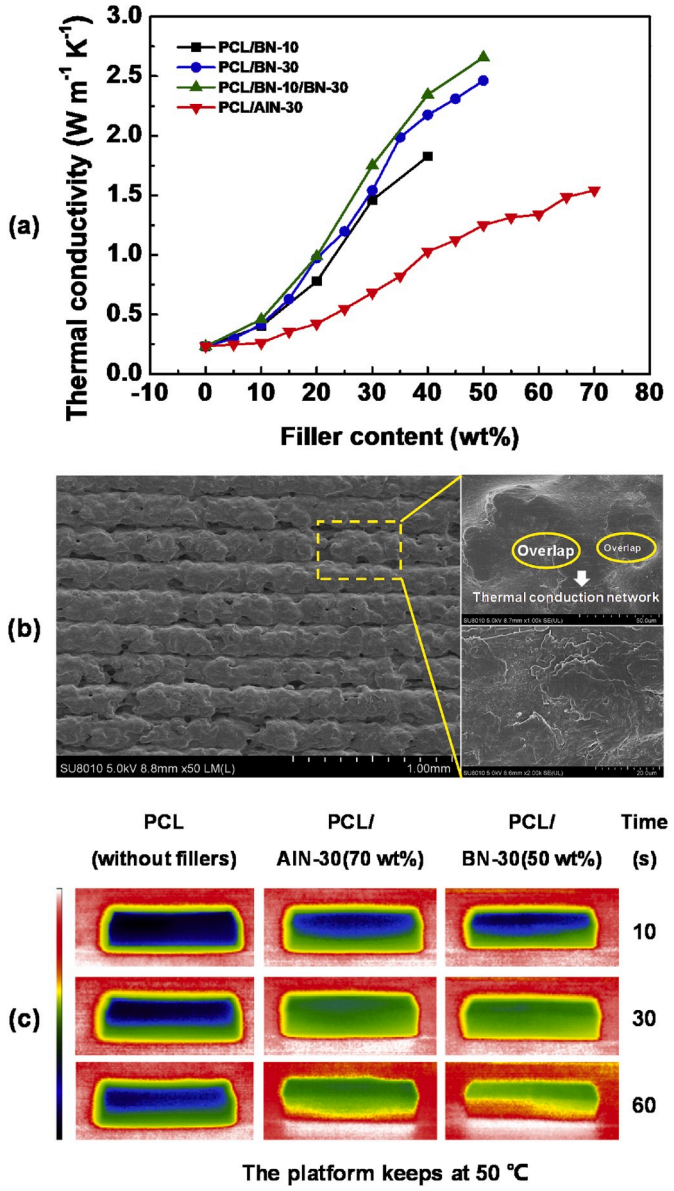

Fig. 2. (a) The effect of filler content on thermal conductivity assessed by the transient hot-wire method. The weight percentage of BN-10 and BN-30 in the PCL/BN-10/BN-30 composites (green spots) is equal (i.e. 1:1), corresponding to Fig. 1a. (b) The SEM micrographs of cross section of printed part. (c) The IRT photos of homogeneous samples with the passage of time (time unit: seconds). (For interpretation of the references to colour in this figure legend, the reader is referred to the Web version of this article.)

Since two high-power step motors of the multicomponent FDM 3D printer can be respectively controlled through software, the proportion of two materials inside one sample can be achieved arbitrarily. The samples with linear variation of proportion between 0 and 100 wt% were prepared to investigate the tendency of thermal conductivity, as illustrated in Fig. 3a–c. Fig. 3d deduced from Fig. 2a indicates the variation of the thermal conductivity versus the number of layer, which reveals that the curve of AlN has a constant slope while the one of BN increases initially and then reduces. The derivation of the latter (the inset in Fig. 3d) shows a peak at $n_L^0 = 16.2$ according to the equation: $\partial\lambda/\partial n_L$, where λ and n_L means the thermal conductivity and the number of layer. It is attributed to that the network of thermal conduction is constructed when the loading of BN particles approaches 27 wt%, leading to a substantial growth in thermal conductivity. The value of 27 wt% (marked by c^0) corresponds to the content of BN particles in PCL/

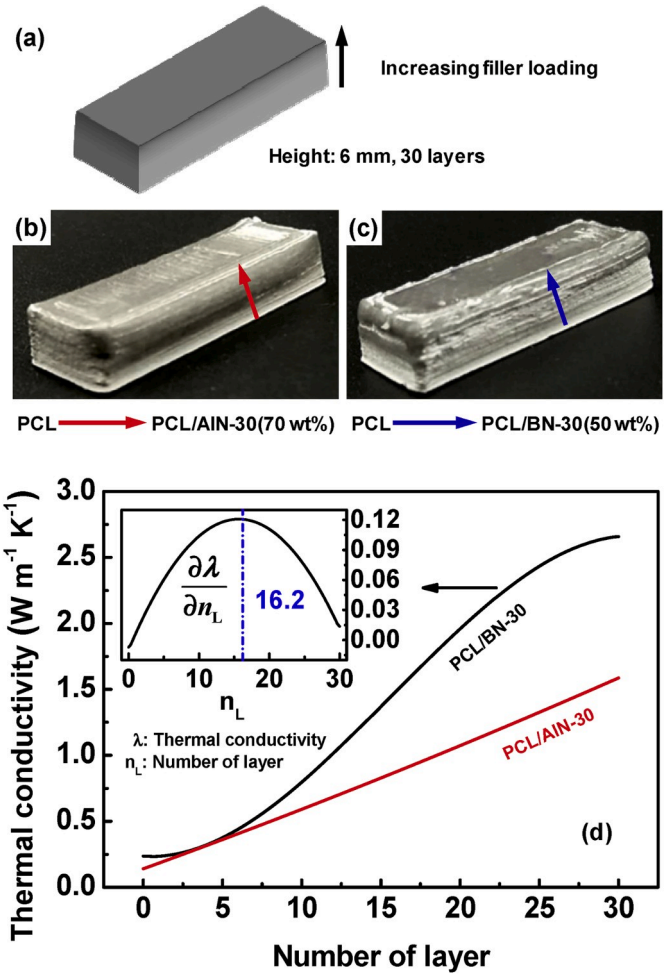

Fig. 3. The (a) sketch and photos of samples with (b) AlN-30 and (c) BN-30. (d) The variation trend of thermal conductivity (λ) with the number of layer (n_L). The inset in (d) shows the differential of thermal conductivity versus number of layer ($\partial\lambda/\partial n_L$) for the PCL/BN-30 composites (black line). The short dash dot line in the inset in (d) locate at the peak (maximum) of $\partial\lambda/\partial n_L$ (≈16.2).

BN-30 nanocomposites at $n_L^0 = 16.2$ (the peak of $\partial\lambda/\partial n_L$) and calculated by

$$c^0 = \frac{n_L^0}{n} \times c$$

where n is the total layers of the BN gradient specimen and c is the content of BN particles of the FDM 3D printing filament. In this study, $n = 30$ and $c = 50$ wt%.

Although the properties of each layer of the thermoplastic functionally gradient composite parts (TFGCPs) by FDM 3D printing are various, it is meaningful to test the thermal conductive properties as a whole part, listed in Table 1. Different from the previous transient hot-wire method adopted for homogeneous parts, the steady-state heat flow is used to evaluate the thermal conductivity of inhomogeneous parts, which is more like the realistic application scenarios, because it takes the whole system into consideration, including heater, cooling unit, and specimen. As observed in Fig. 4a, the thermal conductivity of TFGCPs (D, E, F, and G) lies between the one of pure PCL (A) and homogeneous parts with AlN or BN fillers (B and C), which has been explained before. Also, there is an interesting phenomenon worthy of attention that the thermal conductivity is lower when the side of PCL/fillers in the inhomogeneous parts contacts the cool end (D and F). However, when the side of PCL/fillers contacts the hot end (E and G), the thermal conductivity is 1.448 W m^{-1} K^{-1} (E) and 2.234 W m^{-1} K^{-1} (G), respectively.

Table 1
The type of samples by FDM 3D printing.

Sample ID	Type
A	PCL
B	PCL/AlN-30 (70 wt%)
C	PCL/BN-30 (50 wt%)
D	PCL→PCL/AlN-30 (70 wt%), from bottom to top[a]
E	PCL/AlN-30 (70 wt%)→PCL, from bottom to top
F	PCL→PCL/BN-30 (50 wt%), from bottom to top
G	PCL/BN-30 (50 wt%)→PCL, from bottom to top

[a] The bottom and top side contacts with the hot (heat source) and cool end, respectively.

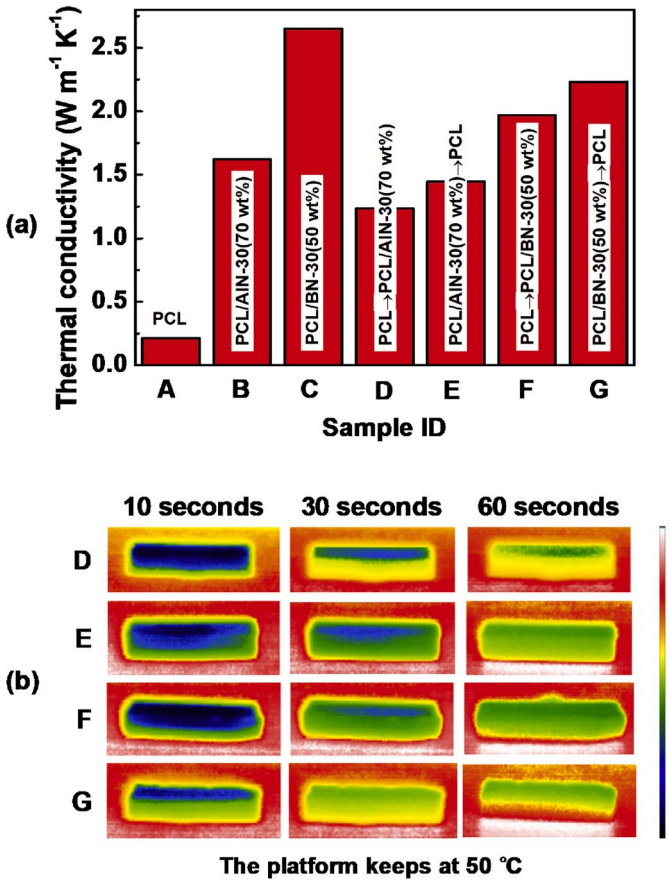

Fig. 4. (a) The thermal conductivity of different FDM 3D-printed parts: Sample A, B, C, D, E, F, and G corresponding to Table 1 (b) The IRT photos of inhomogeneous samples with the passage of time.

The explanation has the relationship with the thermal resistance of specimens. The ordered lattice structures of AlN and BN have much higher efficiency than the lattice vibration that the PCL matrix relies on in thermal conduction. Thus the thermal resistance decreases, leading to less heat loss in terms of the contact of two sides with smaller difference in thermal conductivity. As a result, it takes less time to approach thermal equilibrium of the whole system in E than D or G than F. The IRT photos further manifest the differences in thermal conductivity of inhomogeneous samples, as observed in Fig. 4b.

Based on the above investigations, both the component structure and property parameters of the thermoplastic FGMs show continuous changes, which can improve the material strength in the interface area. Also, both sides of the same materials have different properties or functions, which can achieve matching performance without failure under harsh service conditions. Due to the difference in expansion coefficient between the two materials, huge thermal stress will be generated when used at high temperature, resulting in spalling on the material surfaces and failure of the materials. The thermoplastic FGMs can not only connect two incompatible materials to improve the bonding strength and reduce the residual stress that cracks different materials, but also can relieve the problem effectively and achieve the effect of heat transfer at the same time.

4. Conclusions

The thermoplastic functionally gradient composite parts (TFGCPs) were fabricated by modified multicomponent FDM 3D printing. The thermal conductive properties of TFGCPs were studied by slice and as a whole, which established the relationship between properties and structures of the TFGCPs. The results show that when introducing 70 wt % of AlN-30 (or 50 wt% of BN-30) powders, the thermal conductivity reaches 1.543 (or 2.463) W m^{-1} K^{-1}, comparing to 0.233 W m^{-1} K^{-1} for the pure PCL. The variation curve of the thermal conductivity versus the number of layer reveals that the curve of PCL/AlN composites has a constant slope, while the PCL/BN has a changing slope. It was also discovered that the he thermal conductivity has a relationship with the filler loading direction. This study provides a novel approach and plays an instructive role to prepare TFGCPs by FDM 3D printing, which broadens the application as intermediate layer between two materials with huge difference in thermal expansion coefficient.

Declaration of competing interest

The authors declare that they have no known competing financial interests or personal relationships that could have appeared to influence the work reported in this paper.

CRediT authorship contribution statement

Jianlei Wang: Conceptualization, Methodology, Investigation, Data curation, Writing - original draft. **Suhail Mubarak:** Investigation, Resources, Software, Data curation. **Duraisami Dhamodharan:** Investigation, Validation, Visualization. **Nidhin Divakaran:** Formal analysis, Visualization. **Lixin Wu:** Supervision, Project administration, Funding acquisition. **Xu Zhang:** Data curation, Funding acquisition, Writing - review & editing.

Acknowledgements

This work was financially supported by the Fundamental Research Funds for the Central Universities (Grant No.: 2232020D-11), the State's Key Project of Research and Development Plan (Grant No.: 2016YFB1100900), the National Natural Science Foundation of China (Grant No.: U1905217), the Regional Key Program of Science and Technology Service Network Initiative from Chinese Academy of Sciences (KFJ-STS-QYZX-023), the Key Research Project of Jiangxi Province (Grant No.: 20192ACB80002), the Fund of National Engineering and Research Center for Commercial Aircraft Manufacturing, the Pilot Project of Fujian Province (Grant No.: 2019H0050), the FJIRSM & IUE Joint Research Fund (Grant No.: RHZX-2019-005), the Fund of National Engineering Research Center for Optoelectronic Crystalline Materials, and the Regional Development Projects of Fujian Province (Grant No.: 2018H4027).

Appendix A. Supplementary data

Supplementary data to this article can be found online at https://doi.org/10.1016/j.coco.2020.03.012.

References

[1] D.K. Kim, W. Woo, E.Y. Kim, S.H. Choi, Microstructure and mechanical characteristics of multi-layered materials composed of 316L stainless steel and ferritic steel produced by direct energy deposition, J. Alloys Compd. 774 (2019) 896–907.

[2] J.S. Zuback, T.A. Palmer, T. DebRoy, Additive manufacturing of functionally graded transition joints between ferritic and austenitic alloys, J. Alloys Compd. 770 (2019) 995–1003.

[3] J. Li, Y. Guan, G. Wang, G. Zhao, J. Lin, H. Naceur, D. Coutellier, Meshless modeling of bending behavior of bi-directional functionally graded beam structures, Compos. B Eng. 155 (2018) 104–111.

[4] H. Liu, H. Liu, J. Yang, Vibration of FG magneto-electro-viscoelastic porous nanobeams on visco-Pasternak foundation, Compos. B Eng. 155 (2018) 244–256.

[5] R. Kumar, A. Lal, B.N. Singh, J. Singh, New transverse shear deformation theory for bending analysis of FGM plate under patch load, Compos. Struct. 208 (2019) 91–100.

[6] S. Hong, D. Sycks, H.F. Chan, S. Lin, G.P. Lopez, F. Guilak, K.W. Leong, X. Zhao, 3D printing of highly stretchable and tough hydrogels into complex, cellularized structures, Adv. Mater. 27 (2015) 4035–4040.

[7] Lind Ju, T.A. Busbee, A.D. Valentine, F.S. Pasqualini, H. Yuan, M. Yadid, S.J. Park, A. Kotikian, A.P. Nesmith, P.H. Campbell, J.J. Vlassak, J.A. Lewis, K.K. Parker, Instrumented cardiac microphysiological devices via multimaterial three-dimensional printing, Nat. Mater. 16 (2017) 303–308.

[8] C. Sciancalepore, F. Moroni, M. Messori, F. Bondioli, Acrylate-based silver nanocomposite by simultaneous polymerization–reduction approach via 3D stereolithography, Compos Commun 6 (2017) 11–16.

[9] L. Li, Y. Chen, T. Yu, N. Wang, C. Wang, H. Wang, Preparation of polylactic acid/TEMPO-oxidized bacterial cellulose nanocomposites for 3D printing via Pickering emulsion approach, Compos Commun 16 (2019) 162–167.

[10] V. Tambrallimath, R. Keshavamurthy, D. Saravanabavan, P.G. Koppad, G.S. P. Kumar, Thermal behavior of PC-ABS based graphene filled polymer nanocomposite synthesized by FDM process, Compos Commun 15 (2019) 129–134.

[11] J. Wang, T. Senthil, L. Wu, X. Zhang, Enhancement of lightweight composite parts with robust cellular structures by combining fused deposition modeling and electromagnetic induction heating, Adv. Eng. Mater. 20 (8) (2018), 1800215.

[12] M. Spoerk, C. Savandaiah, F. Arbeiter, G. Traxler, L. Cardon, C. Holzer, J. Sapkota, Anisotropic properties of oriented short carbon fibre filled polypropylene parts fabricated by extrusion-based additive manufacturing, Compos. Appl. Sci. Manuf. 113 (2018) 95–104.

[13] D.I. Chukov, A.A. Stepashkin, F.S. Senatov, A.I. Salimon, A.M. Korsunsky, S. D. Kaloshkin, 3D-printed PEEK-carbon fiber (CF) composites Structure and thermal properties, Compos. Sci. Technol. 164 (2018) 319–326.

[14] X. Tian, T. Liu, C. Yang, Q. Wang, D. Li, Interface and performance of 3D printed continuous carbon fiber reinforced PLA composites, Compos. Appl. Sci. Manuf. 88 (2016) 198–205.

[15] J. Wang, H. Xie, L. Wang, T. Senthil, R. Wang, Y. Zheng, L. Wu, Anti-gravitational 3D printing of polycaprolactone-bonded Nd-Fe-B based on fused deposition modeling, J. Alloys Compd. 715 (2017) 146–153.

[16] D.A. Lados, M.A. Ryder, G.S. Iannacchione, A.M. Peterson, Fabrication and properties of novel polymer-metal composites using fused deposition modeling, Compos. Sci. Technol. 158 (2018) 43–50.

[17] M. Areir, Y.M. Xu, R.R. Zhang, D. Harrison, J. Fyson, E.J. Pei, A study of 3D printed active carbon electrode for the manufacture of electric double-layer capacitors, J. Manuf. Process. 25 (2017) 351–356.

[18] J. Wang, L. Wu, D. Zhuo, Z. Weng, Y. Zhou, CN Patent, 2015. ZL 2015 1 0096056.6.

[19] R. Kato, S. Nakagawa, H. Marubayashi, S. Nojima, Isothermal crystallization kinetics of poly(ε-caprolactone) blocks confined in cylindrical microdomain structures as a function of confinement size and molecular weight, Macromolecules 49 (16) (2016) 5955–5962.

[20] D. Mao, J. Chen, L. Ren, K. Zhang, M.M.F. Yuen, X. Zeng, R. Sun, J.B. Xu, C. P. Wong, Spherical core-shell Al@Al_2O_3 filled epoxy resin composites as high-performance thermal interface materials, Compos. Appl. Sci. Manuf. 123 (2019) 260–269.

[21] J. Liu, W. Li, Y. Guo, H. Zhang, Z. Zhang, Improved thermal conductivity of thermoplastic polyurethane via aligned boron nitride platelets assisted by 3D printing, Compos. Appl. Sci. Manuf. 120 (2019) 140–146.

[22] S.H. Jeong, J.B. Song, K.L. Kim, Y.H. Choi, H. Lee, Enhanced thermal properties of epoxy composite containing cubic and hexagonal boron nitride fillers for superconducting magnet applications, Compos. B Eng. 107 (2016) 22–28.

[23] K. Zhang, P. Tao, Y. Zhang, X. Liao, S. Nie, Highly thermal conductivity of CNF/AlN hybrid films for thermal management of flexible energy storage devices, Carbohydr. Polym. 213 (2019) 228–235.